Supporting Information

A Rational Synthesis of Single Atom Iron–Nitrogen Electrocatalysts for Highly Efficient Oxygen Reduction Reaction

Juanjuan Huo[a,b], Li Lu[b], Ziyan Shen[b], Yan Liu[b], Jiaojiao Guo[b], Quanbing Liu[c]*, Yong Wang[b], Hao Liu[a,b,d]*, Minghong Wu[b]* and Guoxiu Wang[d]*

[a] State Key Laboratory of Advanced Special Steel, Shanghai Key Laboratory of Advanced Ferrometallurgy, Shanghai University, Shanghai 200444, P. R. China

[b] Joint International Laboratory on Environmental and Energy Frontier Materials, School of Environmental and Chemical Engineering, Shanghai University, Shanghai 200444, P. R. China

[c] School of Chemical Engineering and Light Industry, Guangdong University of Technology Guangzhou 510006, China

[d] Centre for Clean Energy Technology, Faculty of Science, University of Technology Sydney Broadway, Sydney, NSW 2007, Australia

Corresponding Authors

***E-mail**: haoliu@shu.edu.cn, mhwu@shu.edu.cn, liuqb@gdut.edu.cn, guoxiu.wang@uts.edu.au.

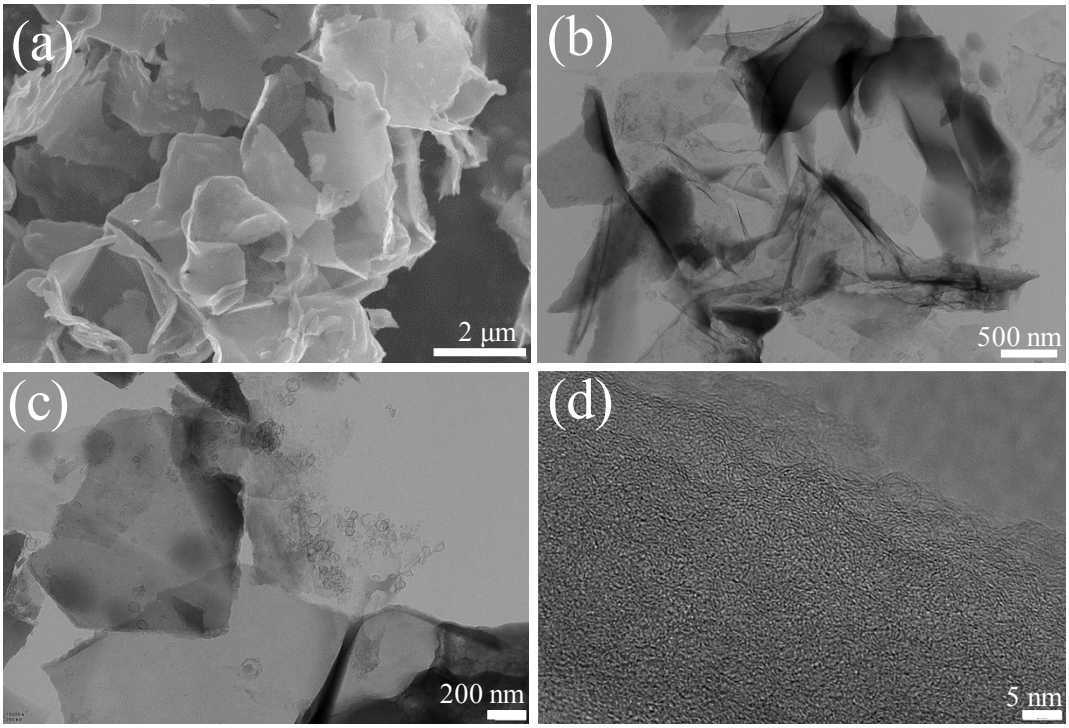

Fig. **S1** (a) SEM image of porous carbon. (b, c and d) Low and high magnification TEM images of porous carbon.

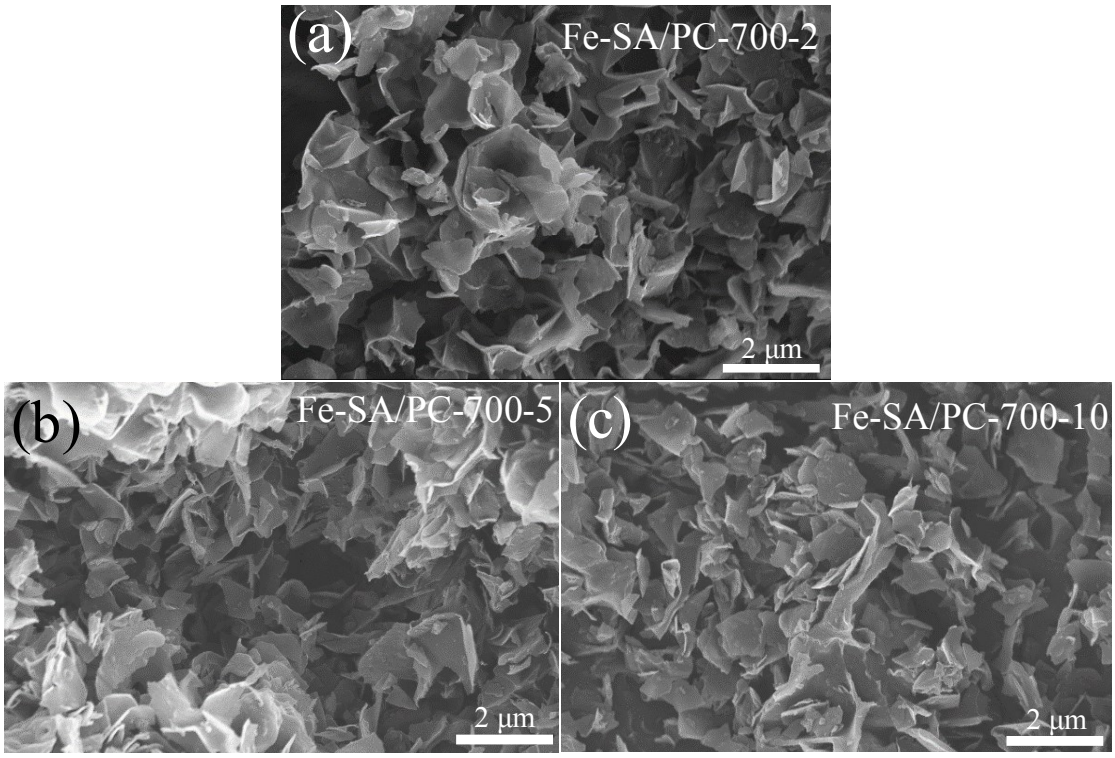

Fig. **S2** SEM images of (a) Fe–SA/PC–700–2, (b) Fe–SA/PC–700–5 and (c) Fe–SA/PC–700–10 samples.

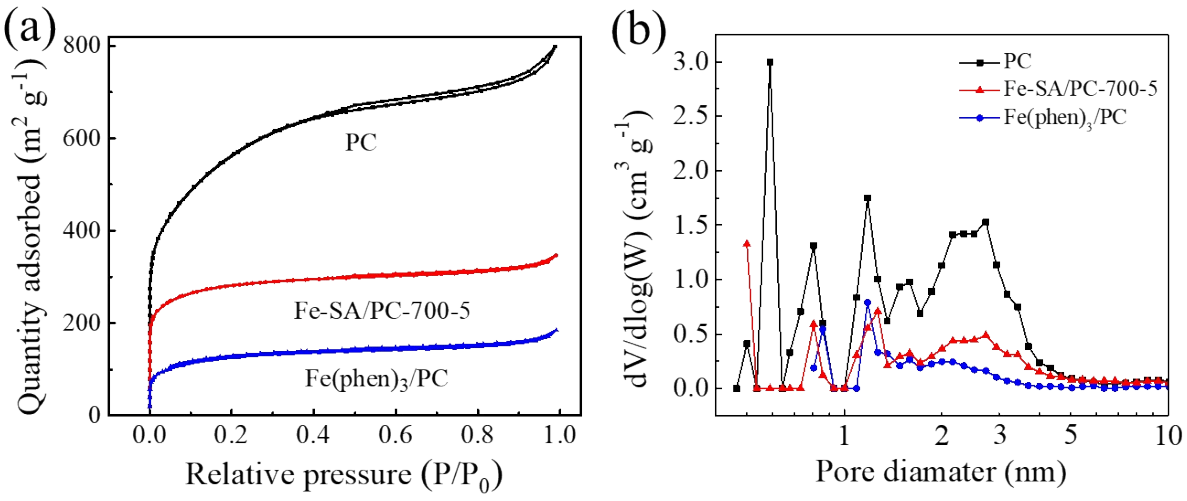

Fig. S3 (a) N_2 adsorption/desorption isotherms of porous carbon, Fe(phen)$_3$/PC and Fe–SA/PC–700–5 samples and (b) the corresponding pore distribution curves.

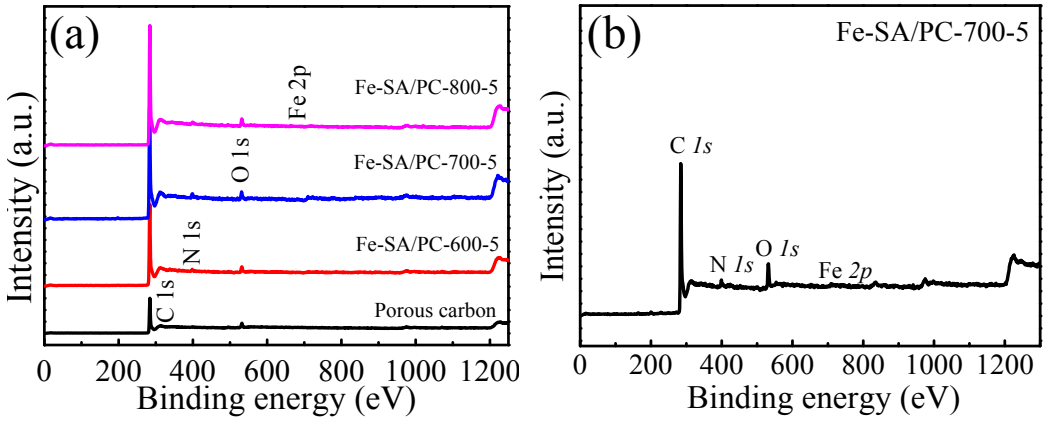

Fig. S4 XPS spectra of as–prepared samples under different temperatures (a) before etching and (b) after etching.

Theoretical calculations for $Fe(phen)_3$ complex adsorption

1.1 Initial structure preparation (Fe:Phen = 1:3) 1,10–phenanthroline iron complex, pristine carbon sheet, carbon nanopore with and without oxygen edges

All structures are constructed using the Materials Studio package version 2018. The initial structures of the pristine carbon sheet, carbon nanopore with and without oxygen edges are as shown in **Fig. S5** The sizes of the model are chosen based on experimental nanopore sizes. The carbon sheet and nanopores are hydrogen terminated for the edges. The oxide edges shown in **Fig. S5 (c)** are chosen based on the initial structure of the nanopore in **Fig. S5 (b)** for the armchair edges of the pore.

1.2 Geometry optimization for (Fe:Phen = 1:3) 1,10–phenanthroline iron complex and its adsorption conformations on pristine carbon, carbon nanopore with and without oxygen edges

The initial adsorption structures are prepared by the Genmer tool of the Molclus package version 1.82.[1] by constraining the 1,10–phenanthroline iron complex around the center of structures in **Fig. S6** without constraining their rotations and z distance from the center. There are around 30 adsorbed conformations generated from the Genmer run for each combination. The size of complex is about 1 nm based on vdW calculation.

We chose recently developed GFN2–xTB package[2, 3] coupled to the Molclus package[1] version 1.8.3 for further optimization and ranking of structures to find lowest energy conformations that will be used for the adsorption study. In the optimization of the adsorbed structures, position constraints set to the hydrogen atoms around the outer edges of the pristine/nanopore carbon structures to avoid additional unphysical distortion due to adsorption of the $Fe(phen)_3$ complex. The convergence criteria for the xTB optimization has been set to that Energy < 5×10^{-5} Ha and Gradient < 1×10^{-3}Ha/Å. Same criteria has been used for the adsorption study. Prior to the adsorption, geometry optimization at the xTB level for the pristine/nanopore carbon structures, as well as the 1,10–phenanthroline iron complex are also performed with the criteria set above.

The adsorption energies have been calculated as $\triangle E_{ads} = E_{all} - E_{substrate} - E_{complex}$, where E_{all} is the total energy of the adsorbed structure, $E_{substrate}$ is the energy of the substrate while $E_{complex}$ is the energy of the $Fe(phen)_3$ complex with adsorbed conformation.

We adopted the calculations at the GFN2–xTB mainly owing to the fact that the adsorption models in this work generally consist around 400 atoms, which is hardly affordable by conventional semi–empirical quantum chemistry methods such as PM7, not mentioning higher level DFT methods. For the validation purpose, we also optimize the structure of the $Fe(phen)_3$ complex at PBE0–GD3BJ/def2SVP level using the Gaussian 16 package and compares it to the xTB optimized geometry.[4]

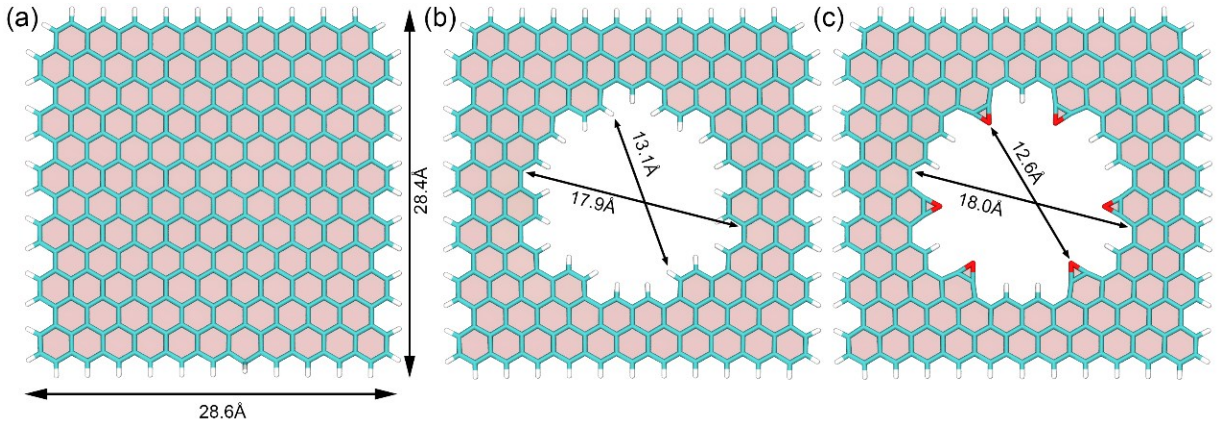

Fig. **S5** The initial structures of (a) pristine carbon sheet (b) carbon nanopore without oxygen edges and (c) carbon nanopore with oxygen edges. Carbon, oxygen and hydrogen atoms are colored in cyan, red and white, respectively.

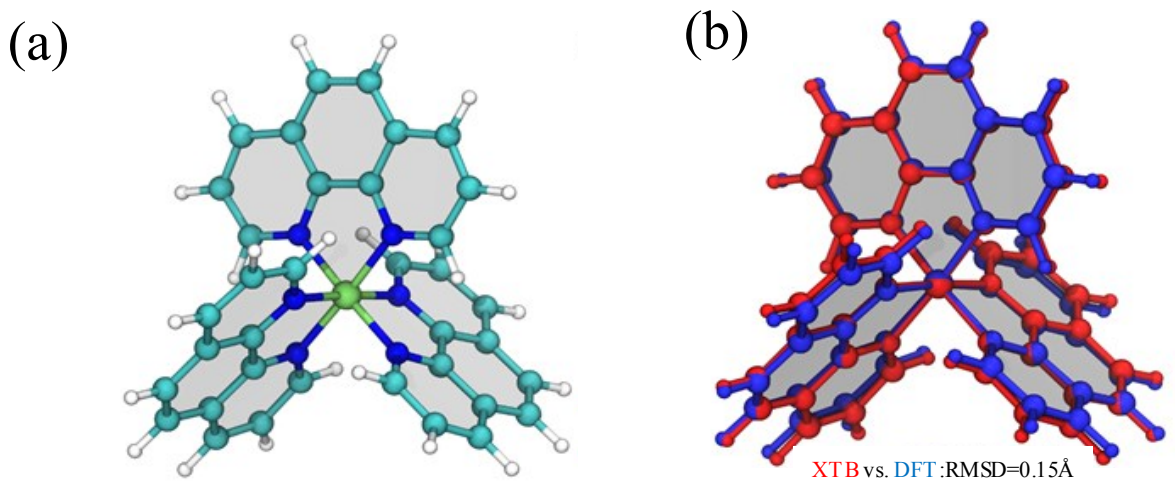

Fig. S6 (a) XTB optimized geometry of the (Fe:Phen=1:3) 1,10–phenanthroline iron complex and (b) overlapped optimized geometry at XTB (red) and DFT (blue, PBE0–GD3BJ/def2SVP) levels. Carbon, nitrogen, iron and hydrogen atoms are colored in cyan, blue, lime, and white, respectively.

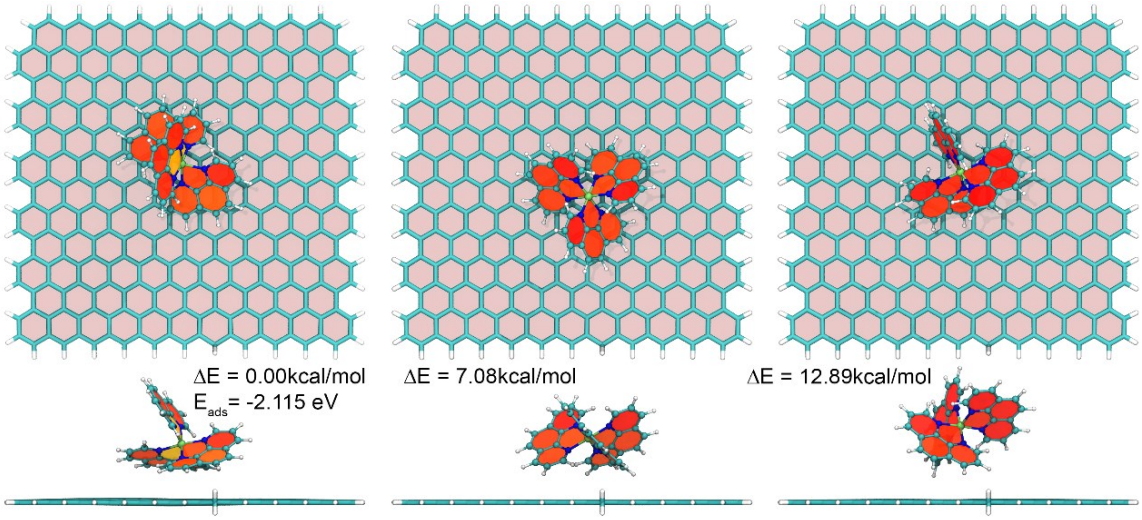

Fig. S7 First three lowest energy XTB optimized geometry of the (Fe:Phen=1:3) 1,10–phenanthroline iron complex adsorbed on pristine carbon sheet. Carbon, nitrogen, iron and hydrogen atoms are colored in cyan, blue, lime, and white, respectively.

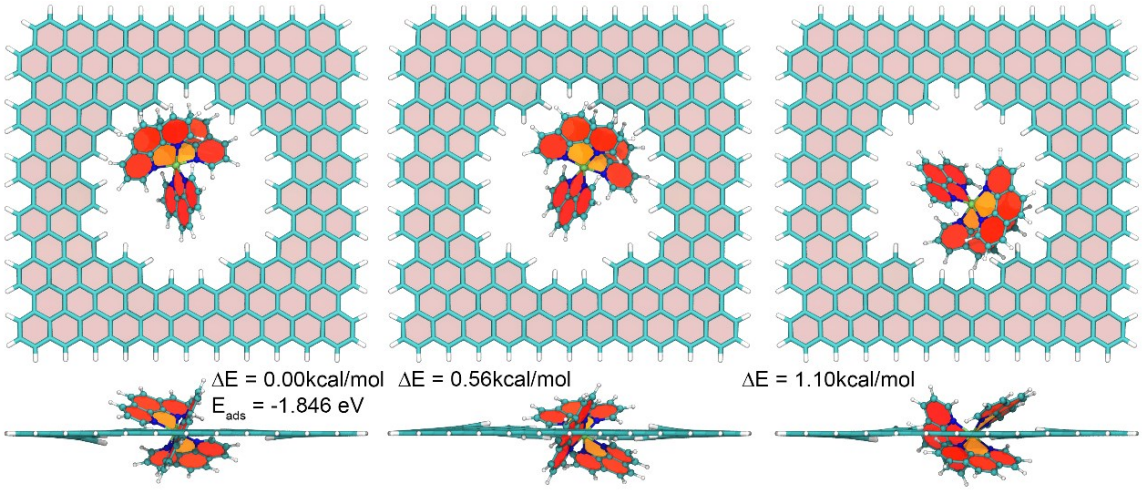

Fig. S8 First three lowest energy XTB optimized geometry of the (Fe:Phen=1:3) 1,10–phenanthroline iron complex adsorbed on nanopore without oxygen edges. Carbon, nitrogen, iron and hydrogen atoms are colored in cyan, blue, lime, and white, respectively.

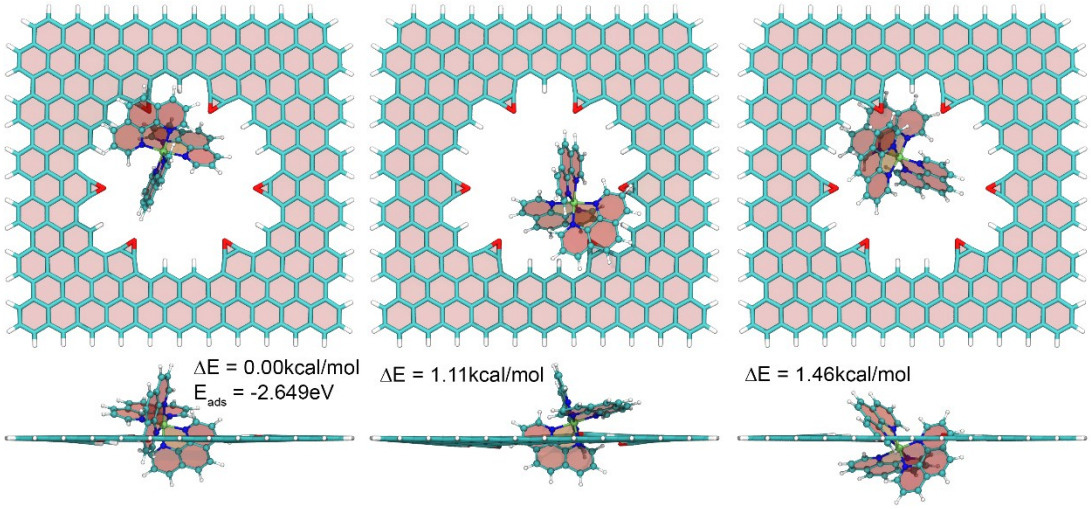

Fig. **S9** First three lowest energy XTB optimized geometry of the (Fe:Phen=1:3) 1,10–phenanthroline iron complex adsorbed on nanopore with oxygen edges. Carbon, nitrogen, oxygen, iron and hydrogen atoms are colored in cyan, blue, red, lime, and white, respectively.

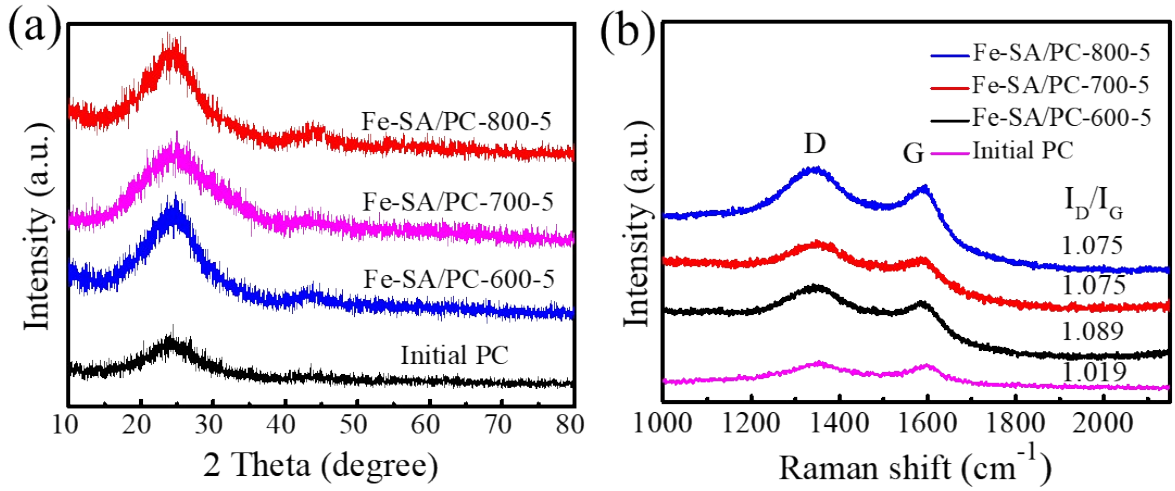

Fig. **S10** (a) XRD patterns and (b) Raman spectra of as–prepared samples.

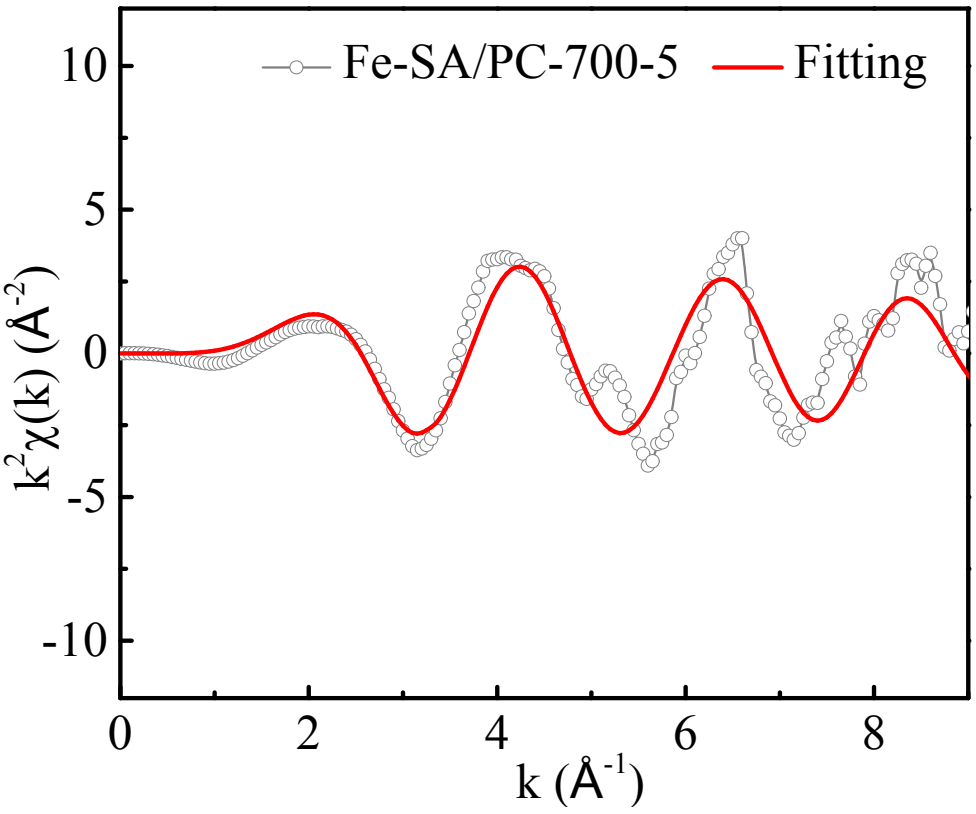

Fig. **S11** The corresponding EXAFS fitting curves of the Fe–SA/PC–700–5 sample at *k* space.

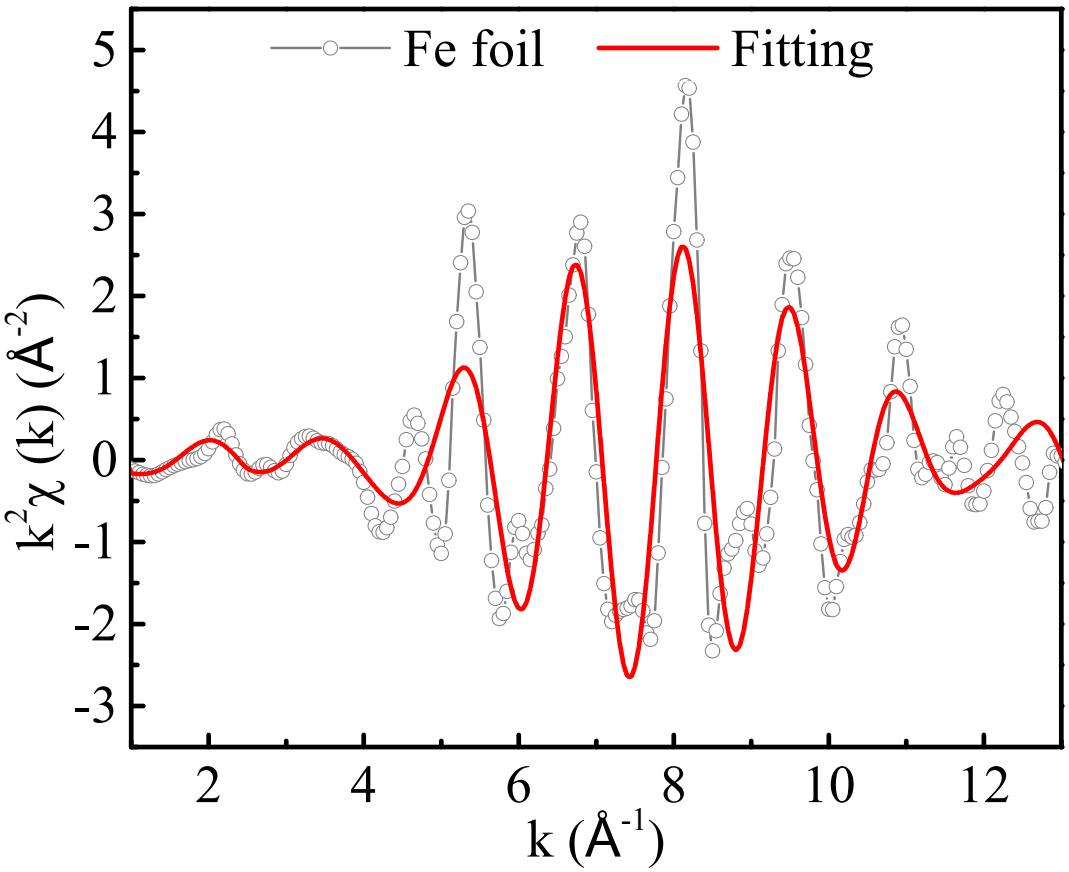

Fig. **S12** The corresponding EXAFS fitting curves of Fe foil at *k* space.

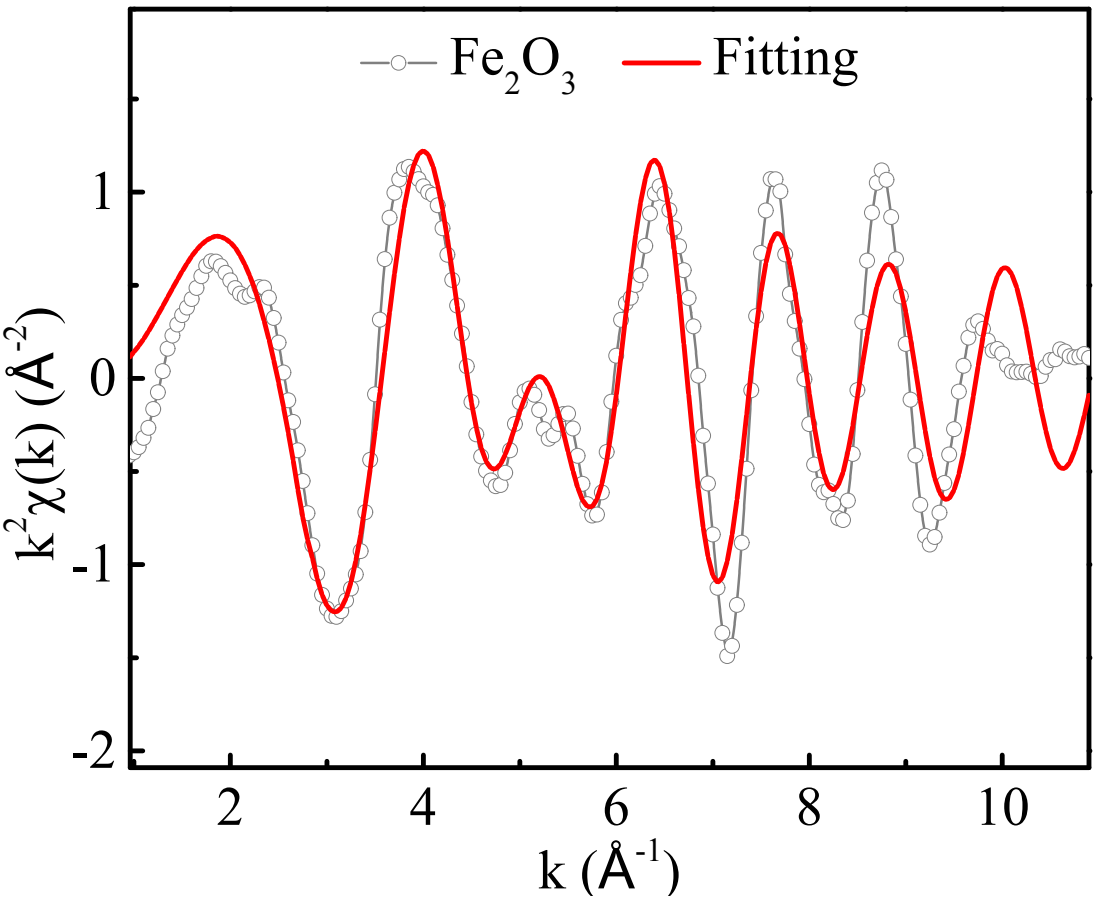

Fig. **S13** The corresponding EXAFS fitting curves of Fe_2O_3 at *k* space.

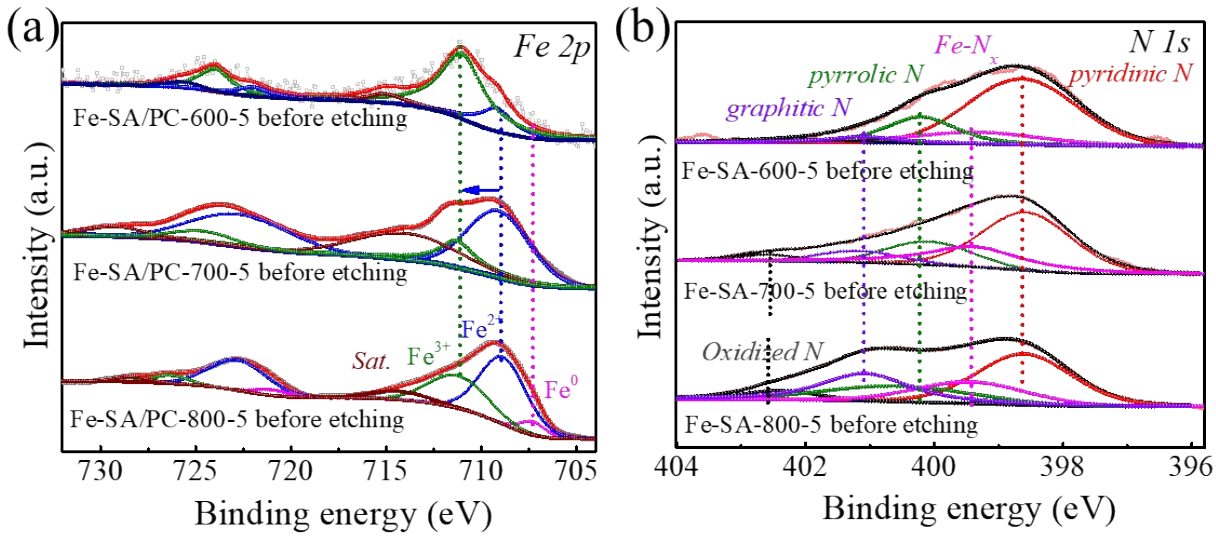

Fig. **S14** High–resolution X–ray photoelectron spectra (XPS) of (a) Fe 2p, and (b) N 1s in Fe–SA/PC–600–5, Fe–SA/PC–700–5, and Fe–SA/PC–800–5 samples before etching.

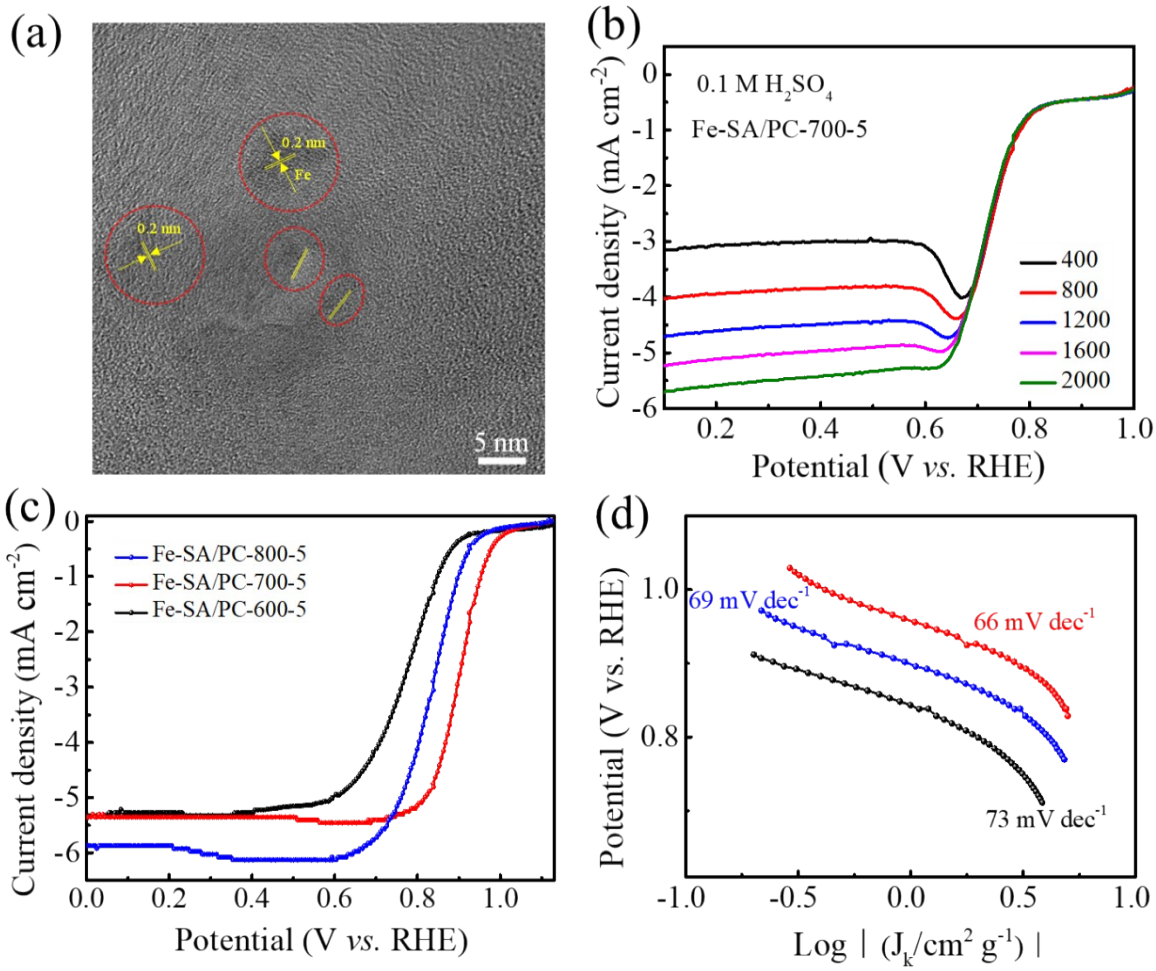

Fig. S15 (a) HRTEM of Fe–SA/PC–800–5 sample, the nanoparticles in red circle can be ascribed to Fe or Fe_3C. (b) LSV curves of Fe–SA/PC–700–5 sample with various rotation rates in 0.1 M H_2SO_4 O_2–saturated solution with a scan rate of 10 mV s^{-1}. (c) LSV curves of Fe–SA/PC–600–5, Fe–SA/PC–700–5 and Fe–SA/PC–800–5 samples in O_2–saturated 0.1 M KOH at 1600 rpm with a scan rate of 10 mV s^{-1} and (d) their corresponding Tafel plots.

It is clear that several small nanoparticles with lattice space of 0.2 nm ascribed to Fe based particles can be obviously observed. Therefore, the poor ORR activity should be contributed to the excessive aggregation of Fe species under higher temperature pyrolysis.

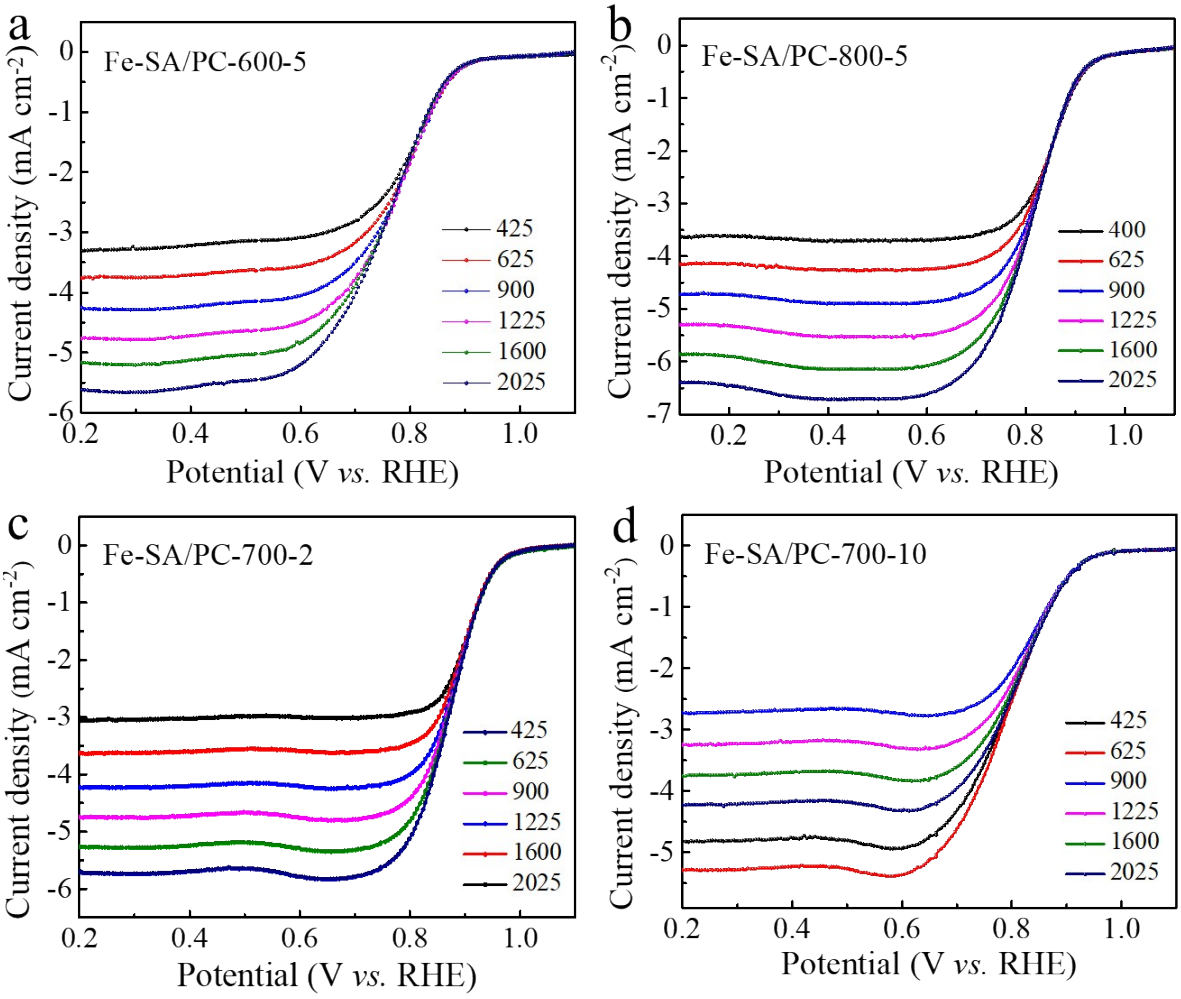

Fig. 16 LSV curves of (a) Fe–SA/PC–600–5, (b) Fe–SA/PC–800–5 catalysts, (c) Fe–SA/PC–700–2 and (d) Fe–SA/PC–700–10 samples in O_2–saturated 0.1 M KOH solution with a scan rate of 10 mV s^{-1} under various rotation speeds.

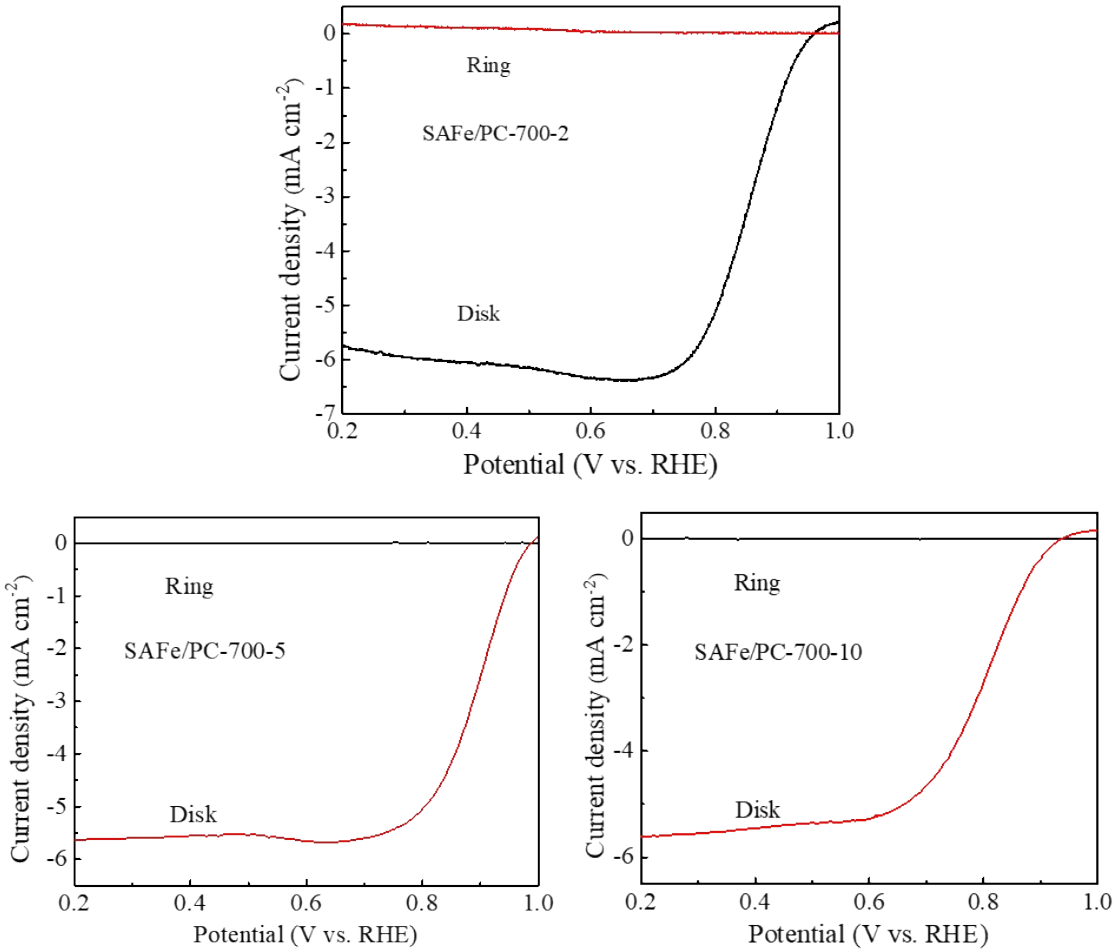

Fig. S17 The corresponding RRDE voltammograms recorded in O_2–saturated 0.1 M of KOH solution at 1600 rpm with a scan rate of 10 mV s^{-1}, and the ring potential was constant at 1.5 V *vs.* RHE.

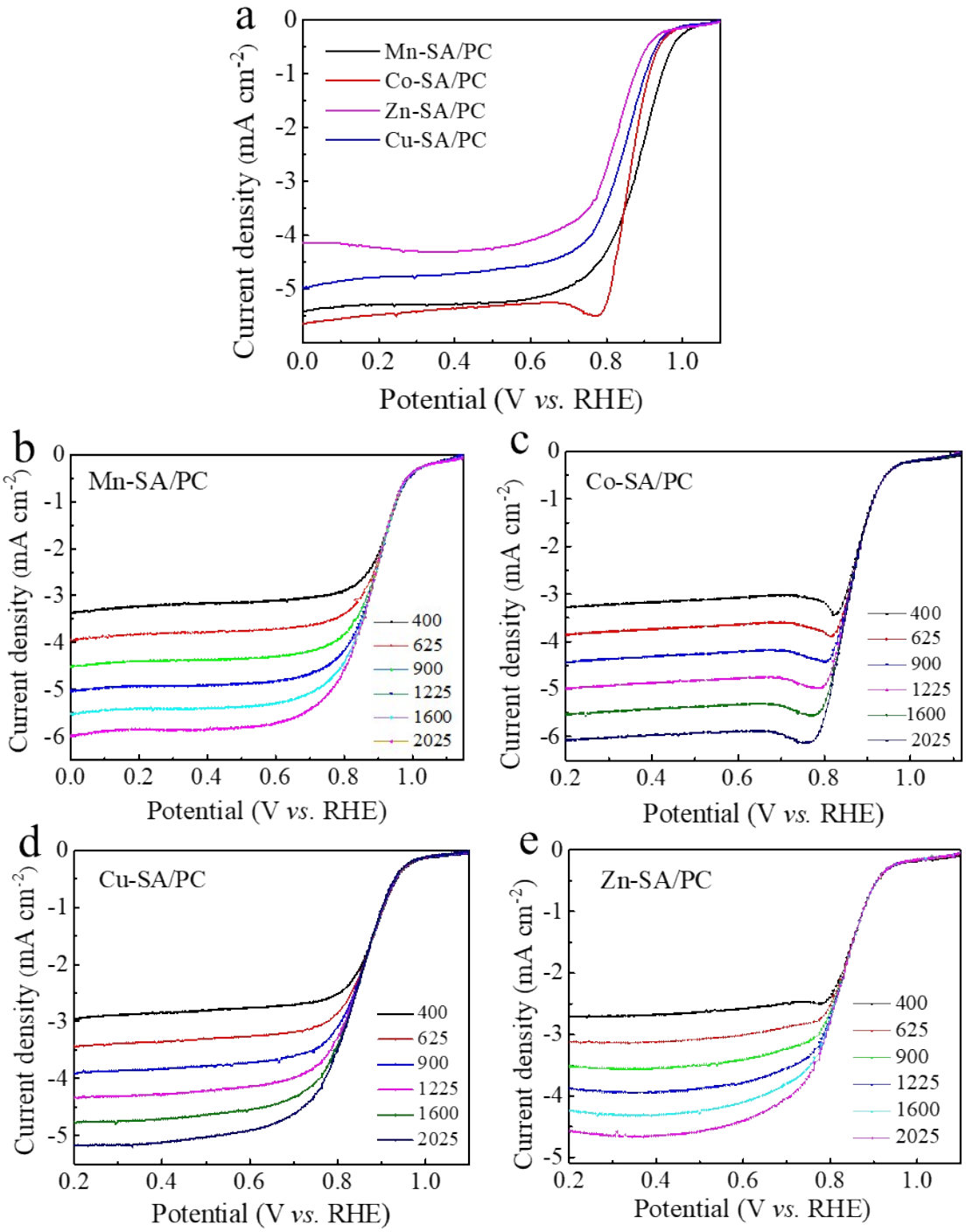

Fig. **S18** (a) LSV curves of as–prepared catalysts toward ORR at 1600 rmp in O_2–saturated 0.1 M KOH solution. (b) Co, (c) Mn, (d) Cu and (e) Zn–based composites prepared by the similar procedure of Fe–SA/PC–700–5 sample at various rotating speed in O_2–saturated 0.1 M KOH solution.

DFT calculations for ORR

The first–principle calculations were performed with the Vienna Ab initio Simulation Package (VASP). The ion–electron interactions were treated with the projected–augmented wave (PAW) method. The exchange–correlation interactions were calculated with the PBE scheme. The energy cut–off was set to 400 eV, and the self–consistent convergence was set at criteria of 0.0001 eV/atom. The spin polarization was considered in the calculation. The structure was constructed based on the monolayer of graphite, and the vacuum layer was about 20 Å。After complete structural optimization, the two structures are presented as follows:

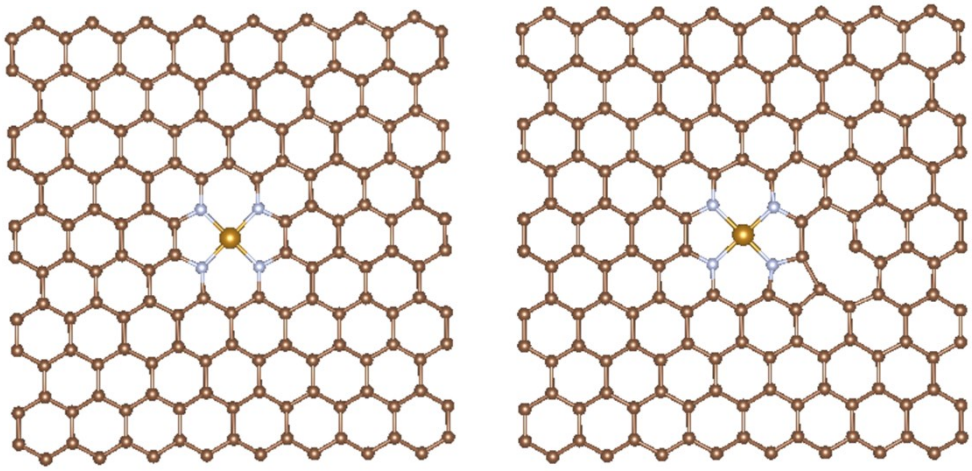

The Norskov's computational hydrogen electrode (CHE) method was applied to calculate the reaction free energy (ΔG) for oxygen reduction reactions (ORR). In the method, with the standard conditions (pH=0, p = 1 bar, T = 298 K), the ΔG of the reaction: $A^* + H^+ + e^- \rightarrow AH^*$, could be calculated from the reaction: $A^* + 1/2H_2 \rightarrow AH^*$, i.e., $\Delta G = G(AH^*) - G(1/2H_2) - G(A^*) + eU'$. Here U is the electrode potential vs. SHE, and in alkaline condition, the formula between U' and U is U' = U + 0.059*(pH).

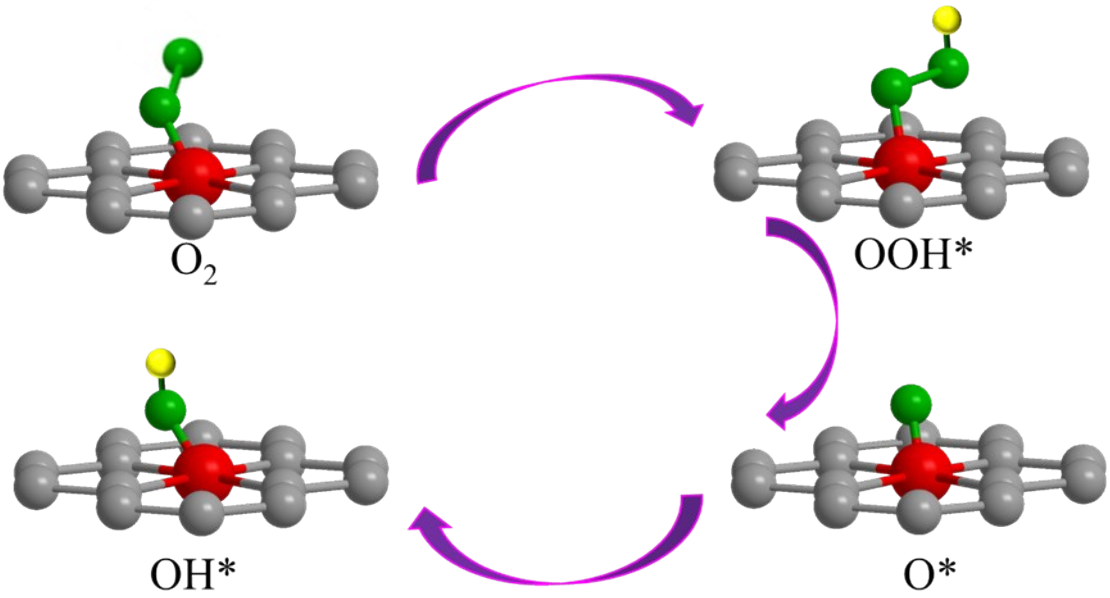

Fig. S19 (a) Geometric structures of the intermediates OOH*, O*, and OH* on Fe–SA/PC.

$$O_2(g) + * \rightarrow O_2^* \quad (1)$$

$$O_2^* + H_2O(l) + e^- \rightarrow OOH^* + OH^- \quad (2)$$

$$OOH^* + e^- \rightarrow O^* + OH^- \quad (3)$$

$$O^* + H_2O(l) + e^- \rightarrow OH^* + OH^- \quad (4)$$

$$OH^* + e^- \rightarrow OH^- + * \quad (5)$$

The reaction pathways of ORR four–step electron transfer process are presented in the above figures.

Table S1. Comparison of the as–prepared porous carbon, $Fe(phen)_3$/PC–700–5 and Fe–SA/PC–700–5 samples.

Samples	BET surface area ($m^2\ g^{-1}$)	Pore volume ($m^3\ g^{-1}$)
porous carbon	1903	1.23
$Fe(phen)_3$/PC	406.7198	0.285791
Fe–SA/PC–700–5	606.9	0.544

Table S2. The elemental quantification analysis of O and different N species of the obtained catalysts.

Samples	O (at%)	N (at. %)
Fe–SA/PC–600–5	3.72	2.15
Fe–SA/PC–700–5	3.18	3.48
Fe–SA/PC–800–5	2.15	1.82
Porous carbon	6.06	0

Table S3. Parameters of the Fe K–edge EXAFS Fitting results.

Sample	Path	C.N.	R (Å)	$\sigma^2\times10^3$ ($Å^2$)	ΔE (eV)	R factor
Fe foil	Fe–Fe	8*	2.45	1.9	2.5	0.004
	Fe–Fe	6*	2.85	2.5	3.5	
Fe_2O_3	Fe–O	5.6	2.02	12.2	0.7	0.014
	Fe–Fe	4.8	2.97	3.9		
Fe–SA/PC–700–5	Fe–N	4.5	2.00	7.2	1.8	0.006

Table S4. The prepared conditions and performances of as–prepared catalysts in our work.

Catalyst	Fe atomic% in samples (XPS analysis)	Pyrolysis temperature	$E_{(1/2)}$ *vs.* RHE	J_d	Tafel slope
Fe–SA/PC–700–5	0.73 %	700 ^oC	0.91 V	5.4 mA cm^{-2}	66 mV dec^{-1}
Fe–SA/PC–700–2	--	700 ^oC	0.88 V	5.4 mA cm^{-2}	68 mV dec^{-1}
Fe–SA/PC–700–10	--	700 ^oC	0.8 V	4.75 mA cm^{-2}	77 mV dec^{-1}
Fe–SA/PC–600–5	0.71 %	600 ^oC	0.77 V	5.2 mA cm^{-2}	73 mV dec^{-1}
Fe–SA/PC–800–5	1.49 %	800 ^oC	0.83 V	6.1 mA cm^{-2}	69 mV dec^{-1}
NPC	0	700 ^oC	0.75 V	3.78 mA cm^{-2}	80 mV dec^{-1}

Table S5. Comparison of the ORR activities with other previous reports about non–precious metal–based catalysts.

Catalysts	Half–wave potential (V *vs.* RHE)	Electrolyte	Reference
Fe–SA/PC–700–2	**0.88**	0.1 M KOH	**This work**
Fe–SA/PC–700–5	**0.91**	0.1 M KOH	
Fe–SA/PC–700–10	**0.8**	0.1 M KOH	
NGM–Co	0.82	0.1 M KOH	[5]
Co–N_X/C NRA	0.88	0.1 M KOH	[6]
Co–N,B–CSs	0.83	0.1 M KOH	[7]
FeNx–PNC	0.86	0.1 M KOH	[8]
Fe_2–Z_8–C	0.87	0.1 M KOH	[9]
Fe–NGM/C–Fe SAC	0.86	0.1 M KOH	[10]
Fe SAs/PTF–600	0.87	0.1 M KOH	[11]
S, N–Fe/N/C–CNT	0.85	0.1 M KOH	[12]
Fe–N/C–700	0.84	0.1 M KOH	[13]
Fe–N/C catalyst	0.81	0.1 M KOH	[14]
p–Fe–N–CNFs	0.82	0.1 M KOH	[15]
Fe–NGM/C–Fe SAC	0.86	0.1 M KOH	[16]
Fe–ISAs/CN	0.90	0.1 M KOH	[17]

Table S6. Summarized the ORR performance of other as–prepared non–precious metal–based catalysts in this paper.

Catalyst	Fe–SA/PC–700–5	Mn–SA/PC–700–5	Co–SA/PC–700–5	Cu-SA/PC–700–5	Zn–SA/PC–700–5
$E_{(1/2)}$	0.91 V	0.89 V	0.87 V	0.85 V	0.82 V
J_d	5.4 mA cm^{-2}	5.35 mA cm^{-2}	5.4 mA cm^{-2}	4.75 mA cm^{-2}	4.25 mA cm^{-2}

References

[1] T. Lu, Molclus program, Version 1.8.3, http://www.keinsci.com/research/molclus.html, (accessed July–20, 2019).

[2] S. Grimme, C. Bannwarth and P. Shushkov, *J. Chem. Theory Comput*., 2017, **13**, 1989.

[3] C. Bannwarth, S. Ehlert and S. Grimme, *J. Chem. Theory Comput*., 2019, **15**, 1652.

[4] M. J. Frisch, G. W. Trucks, H. B. Schlegel, G. E. Scuseria, M. A. Robb, J. R. Cheeseman, G. Scalmani, V. Barone, G. A. Petersson, H. Nakatsuji, X. Li, M. Caricato, A. V. Marenich, J. Bloino, B. G. Janesko, R. Gomperts, B. Mennucci, H. P. Hratchian, J. V. Ortiz, A. F. Izmaylov, J. L. Sonnenberg, Williams, F. Ding, F. Lipparini, F. Egidi, J. Goings, B. Peng, A. Petrone, T. Henderson, D. Ranasinghe, V. G. Zakrzewski, J. Gao, N. Rega, G. Zheng, W. Liang, M. Hada, M. Ehara, K. Toyota, R. Fukuda, J. Hasegawa, M. Ishida, T. Nakajima, Y. Honda, O. Kitao, H. Nakai, T. Vreven, K. Throssell, J. A. Montgomery Jr., J. E. Peralta, F. Ogliaro, M. J. Bearpark, J. J. Heyd, E. N. Brothers, K. N. Kudin, V. N. Staroverov, T. A. Keith, R. Kobayashi, J. Normand, K. Raghavachari, A. P. Rendell, J. C. Burant, S. S. Iyengar, J. Tomasi, M. Cossi, J. M. Millam, M. Klene, C. Adamo, R. Cammi, J. W. Ochterski, R. L. Martin, K. Morokuma, O. Farkas, J. B. Foresman and D. J. Fox, 2009, Gaussian 09, Revision A.02, Gaussian, Inc., Wallingford CT.

[5] S. Liu, Z. Wang, S. Zhou, F. Yu, M. Yu, C. Y. Chiang, W. Zhou, J. Zhao and J. Qiu, *Adv. Mater*., 2017, **29**, 1700874.

[6] I. S. Amiinu, X. Liu, Z. Pu, W. Li, Q. Li, J. Zhang, H. Tang, H. Zhang and S. Mu, *Adv. Funct. Mater*., 2018, **28**, 1704638.

[7] Y. Guo, P. Yuan, J. Zhang, Y.; Hu, I. S. Amiinu, X. Wang, J. Zhou, H. Xia, Z. Song, Q. Xu, S. Mu, *ACS Nano*, 2018, **12**, 1894.

[8] L. Ma, S. Chen, Z. Pei, Y. Huang, G. Liang, F. Mo, Q. Yang, Jun Su, Y. Gao, J. Zapien, C. Zhi, *ACS Nano*, 2018, **12**, 1949.

[9] Q. Liu, X. Liu, L. Zheng, J. Shu, *Angew. Chem. Int. Ed*., 2018, **57**, 1204.

[10] C. Wang, H. Zhang, J. Wang, Z. Zhao, J. Wang, Y. Zhang, M. Cheng, H. Zhao and J. Wang, *Chem. Mater*., 2017, **29**, 9915.

[11] J. Yi, R. Xu, Q. Wu, T. Zhang, K. Zang, J. Luo, Y. Liang, Y. Huang, R. Cao, *ACS Energy Lett*., 2018, **3**, 883.

[12] P. Chen, T. Zhou, L. Xing, K. Xu, Y. Tong, H. Xie, L. Zhang, W. Yan, W. Chu, C. Wu, Y. Xie, *Angew. Chem. Int. Ed*., 2017, **56**, 610.

[13] Z. K Yang, L. Lin, A. Xu, *Small*, 2016, **12**, 5710.

[14] L. Lin, Q. Zhu, A. Xu, *J. Am. Chem. Soc*., 2014, **136**, 11027.

[15] B. Hu, Z. Wu, S. Chu, H. Zhu, H. Liang, J. Zhang, S. Yu, *Energy Environ. Sci*., 2018, **11**, 2208–2215.

[16] C. Wang, H. Zhang, J. Wang, Z. Zhao, J. Wang, Y. Zhang, M. Cheng, H. Zhao and J. Wang, *Chem. Mater*., 2017, **29**, 9915.

[17] Y. Chen, S. Ji, Y. Wang, J. Dong, W. Chen, Z. Li, R. Shen, L. Zheng, Z. Zhuang, D. Wang, Y. Li, *Angew. Chem. Int. Ed*., 2017, **129**, 7041.